Negative extensibility metamaterials: Occurrence and design-space topology

Eduard G. Karpov, Larry A. Danso, and John T. Klein

Phys. Rev. E **96**, 023002 — Published 7 August 2017

DOI: 10.1103/PhysRevE.96.023002

Negative Extensibility Metamaterials – Occurrence and Design Space Topology

Eduard G. Karpov[*]*, Larry A. Danso, John T. Klein*

Civil & Materials Engineering, University of Illinois at Chicago,

842 W Taylor St, Chicago, IL 60612

Abstract

A negative extensibility material structure pulls back and contracts when the external tensile load reaches certain critical level. In this paper, we reveal basic mathematical features of the nonlinear strain energy function responsible for this unusual mechanical property. A systematic discussion leads to a comprehensive phase diagram in terms of design parameters for a simple unit cell structure that provides a panoramic view of all possible nonlinear mechanical behaviors. A negative extensibility region is clearly identified on the diagram. The sought property is seen to be rare, occurring only for a very narrow range of the design parameters. Nonetheless, due to simplicity of the studied structure we suggest that the negative extensibility should be a more common phenomenon than previously thought. It can appear in simple *bistable* cells made of only several linearly elastic links, although at some peculiar combinations of their properties. These bistable unit cells can be used to design periodic mechanical metamaterials whose examples are shown, as well as innovative architectural metastructures.

Keywords: mechanical metamaterial, bistability, negative extensibility

1. Introduction

Mechanical and structural metamaterials [1-18] are associated with reversal of basic mechanical properties in quasistatic loading cycles. In particular, auxetic metamaterials [6-9] demonstrate negative Poisson ratio, while for origami-based metamaterials [10-12], negative Poisson ratio and negative bending and twisting stiffnesses can be analytically expressed or numerically observed. Motter and Nicolaou [15-16] also showed a possibility for engineered materials with a longitudinal negative compressibility/extensibility property that would contract in the direction of applied tensile load, Fig.1. The same authors suggested that such a contraction may only occur in an abrupt manner because of destabilization of the materials internal structure at the unit cell level when the external load exceeds some threshold value. Chen and Karpov [17] discussed an essential *bistable* nature of negative extensibility structures and metamaterials, whose forward and reverse transitions can be viewed as a polymorphic phase transformation at the microscopic scale. Such a solid-to-solid condensation process is reminiscent of a superelastic phase transition

[*] Corresponding author. Email: ekarpov@uic.edu

and it is accompanied by abrupt energy release in the structure. Two microstructural polymorphs exhibit different stiffnesses, and therefore two different stable states of equilibrium are possible for a same external load. This behavior implies a hysteretic response of the material to periodic loads [15-17].

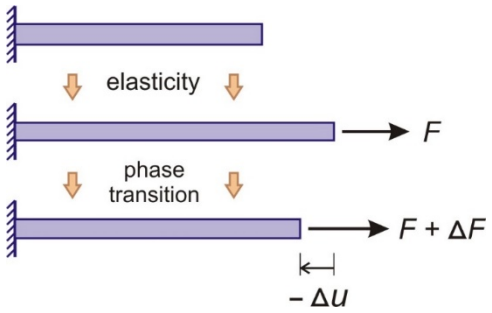

Fig.1: Concept of the longitudinal negative extensibility. Elastically deformed material contracts abruptly in the direction opposite to the force load, when the load reaches a critical value inducing a polymorphic phase transition. Effective elastic modulus and mechanical extensibility ($-\Delta u/\Delta F$) at a constant temperature are negative around the transition point.

A representative potential or strain energy function written for a repetitive unit cell structure of a negative extensibility metamaterial must possess rather exotic mathematical properties, which have not been understood clearly yet. In this paper, we discuss a path toward practical negative extensibility metamaterials via the study of macroscopic structural composites – periodical arrangements of unit cells featuring bistable mechanical hysteresis. These cells are made of *linearly* elastic springs and bars only and they can have their own interesting applications as mechanical actuators, earthquake and explosion impact superdampers, or reconfigurable civil infrastructure components. Furthermore, once important mathematical criteria are understood and many practical examples of these structural metamaterials are demonstrated in the first place, the knowledge gained will facilitate design of negative extensibility in materials at the atomic scale.

From the known cases [15-17] it is clear that a representative (unit) cell of a periodic negative extensibility metastructure may have several degrees of freedom, including at least one internal degree of freedom, even for the case of chain-like models. A systematic stability analysis of such unit cells featuring an essential material or/and geometrical nonlinearity, leading to a bistable hysteretic response, is highly challenging.

In this paper, we rely on geometrical nonlinearity only and discuss an approach to elucidate many necessary features of the potential energy function and to provide practical guidelines toward negative extensibility phenomenon in a macroscopic metastructure made of linearly elastic elements only. A practical mechanical metamaterial would employ this metastructure as a main phase, as well as damping elements, since the negative extensibility transitions are known to be accompanied by release of large amounts of kinetic energy [17]. Thus, we focus on simple bistable unit cells that can potentially be arranged in periodic arrays, and that can be made using

only the following non-buckling element types: (a) linear springs or strings allowing for large deformation described by the engineering strain,

$$\varepsilon = \frac{l-l_0}{l_0} \tag{1}$$

(b) linear elastic bars at moderate deformation measured with the Green's strain,

$$\varepsilon_G = \frac{l^2-l_0^2}{2l_0^2} \tag{2}$$

and (c) rigid pivoted links with no strain. Potential energy of deformation of the spring and bar elements gives, respectively,

$$\pi_\mathrm{s} = \frac{k_\mathrm{s}}{2} l_0^2 \varepsilon^2 = \frac{k_\mathrm{s}}{2}(l-l_0)^2 \tag{3}$$

$$\pi_\mathrm{b} = \frac{k_\mathrm{b}}{2} l_0^2 \varepsilon^2 \approx \frac{k_\mathrm{b}}{2} l_0^2 \varepsilon_G^2 = \frac{k_\mathrm{b}}{8l_0^2}(l^2-l_0^2)^2 \tag{4}$$

where k, l_0 and l are the stiffness, relaxed and deformed lengths of the elements. The bar's stiffness is $k_\mathrm{b} = EA/l_0$, in terms of its Young's modulus E and cross section area A. Equation (4) represents the only approximation adopted in the analysis, and it is good at moderate strains in the bars (< 0.05), because $\varepsilon_G = \varepsilon + \varepsilon^2/2$.

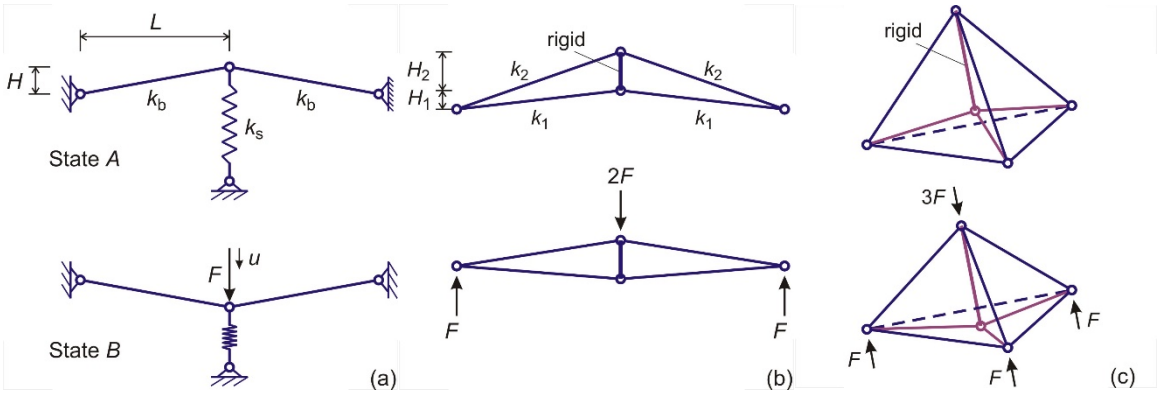

Fig.2: Examples of bistable structures with one independent degree of freedom. Parameters k are linear stiffnesses of the spring or bar elements.

The strain energies (3-4) will lead to quartic (bistable) potentials for the structure's representative unit cells, whose mathematical stability analysis is tractable. In the simplest case of Fig.2a structure with one independent degree of freedom, we may write the total potential energy as

$$\Pi = \frac{k_\mathrm{b}}{4(L^2+H^2)}(u^2-2Hu)^2 + \frac{1}{2}k_\mathrm{s}u^2 - Fu \tag{5}$$

where k_b and k_s are the bar and spring stiffnesses respectively. This expression can be written in a dimensionless form,

$$U = x^4 - ax^3 + bx^2 - fx \tag{6}$$

$$f = \frac{4(L^2+H^2)}{H^3}\frac{F}{k_b}, \quad U = \frac{f}{H}, \quad x = \frac{u}{H}, \quad a = 4, \quad b = 4 + \frac{2(L^2+H^2)k_s}{k_b H^2} \tag{7}$$

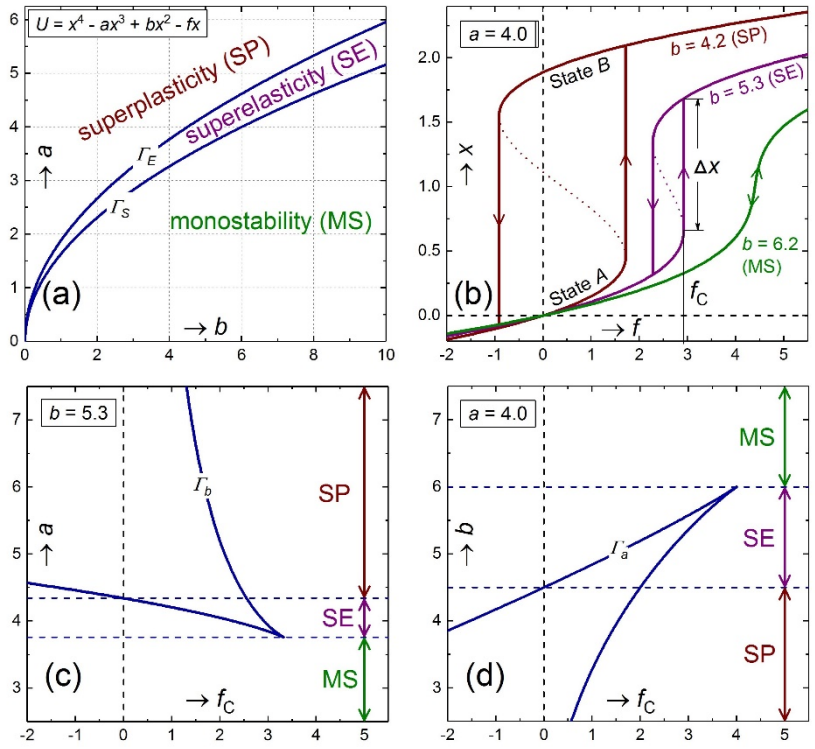

Fig.3: (a) Phase diagram of the generic system governed by the quartic potential $U = x^4 - ax^3 + bx^2 - fx$. (b) Three possible types of the mechanical response: structural monostability (MS) or usual geometrical nonlinearity, bistable superelasticity (SE), and bistable superplasticity (SP) when recovery of structural deformation requires load reversal. Switching between the states *A* and *B* occurs at a critical load $f = f_C$. Superelastic strain due to the transition ε_{SE} is proportional to Δx. (c-d) Stability diagrams showing values of the critical forces f_C at specific values of the system parameters *a* and *b*.

A similar potential energy expression (6) can also be written for Fig.2b structure, although using its own dimensionless parameters,

$$f = \frac{L^2+H_2^2}{H_1^3(1+\gamma)}\frac{F}{k_2}, \quad U = \frac{f}{H_1}, \quad x = \frac{u}{H_1}, \quad a = \frac{H_2+\gamma H_1}{H_1(1+\gamma)}, \quad b = \frac{H_2^2+\gamma H_1^2}{H_1^2(1+\gamma)} \tag{8}$$

where $\gamma = \frac{L^2+H_2^2}{L^2+H_1^2}\frac{k_1}{k_2}$. In equations (6-8), the dimensionless load *f* is an external *control* parameter, the dimensionless displacement *x* is a *state* parameter describing the state of deformation, and the

coefficients a and b are the *system* or *design* parameters. This terminology is typical for catastrophe theory [20-22], where design parameters of this type, though, may serve the role of control parameters since they define a desired system behavior. Note that Fig.2a structure has only one independent design parameter, since the value a cannot vary in (7). Discussion of Fig.2c structure and other examples leading to the potential energy form (6) can be found in [19]. A *phase diagram* of the generic system governed by (6) can be constructed for the system parameters a and b, and it is shown in Fig.3a. Here, three basic types of the mechanical response are possible. One of them is monostable and two are *bistable* – when two stable equilibrium configurations are possible for a same load. The bistable (hysteretic) response can be either *structural superelasticity* or *structural superplasticity* [19] depending on whether the initial configuration is recovered upon load removal. The term superplasticity implies that a full recovery of the overall (structural) plastic deformation is still possible upon load reversal, see Fig.3b.

The bottom line in the phase diagram, Fig.3a, represents the onset of bistability because all designs above this line are bistable and all those below are monostable. This line is a locus of points $\{a, b\}$ that represent simultaneously a mechanical equilibrium, destabilization (zero stiffness) and an undulation point or cusp singularity [19-22] of the potential:

$$U'_x = U''_{xx} = U'''_{xxx} = 0: \qquad 3a^2 - 8b = 0 \tag{8}$$

The upper curve in Fig.3a diagram represents designs where the reverse destabilization and transition $B \rightarrow A$ occurs at a zero load. These design points must satisfy the condition:

$$U'_x = U''_{xx} = 0 \ \wedge \ f = 0: \qquad 9a^2 - 32b = 0 \tag{9}$$

The *stability diagrams* of Fig.2c and Fig.2d show the critical loads, $f = f_C$, at which structural destabilization will occur at given system parameters. The curves shown were plotted parametrically by fixing either b or a and using x as a running variable,

$$U'_x = U''_{xx} = 0: \qquad \begin{cases} f_C = x(b - 2x^2), \ a = b/3x + 2x \\ f_C = x^2(3a - 8x), \ b = 3x(a - 2x) \end{cases} \tag{10}$$

As can be seen, Fig.3 diagrams provide a panoramic view of all possible basic types of mechanical behavior in the bistable systems of Fig.2 type. These diagrams also enable design of a specific desired behavior, as well as magnitudes of the critical loads associated with the forward and reverse transitions of the system. We note that negative extensibility is not observed yet in the simplest bistable cells, as in Fig.2, which can be described by the potential (6) and Fig.3a phase diagram. Apparently, negative compressibility requires a more complex form of bistability involving a greater number of independent degrees of freedom per unit cell.

Motter and Nicolaou [15] and also Chen and Karpov [17] provided a good reasoning that the sought negative extensibility behavior must arise from at least one or more additional independent *internal* degrees of freedom in a representative unit cell of the metamaterial. In this paper, we suggest that systematic studies of such bistable unit cells could employ analytical reasoning similar to equations (1-7), strengthened by numerical solution of nonlinear algebraic equations of the type (8-10). We will derive a generic potential energy form for a class of

bistable structures with two independent degrees of freedom, including one internal degree of freedom, followed by a phase diagram derivation and demonstration of the negative extensibility property at a certain combination of the system parameters.

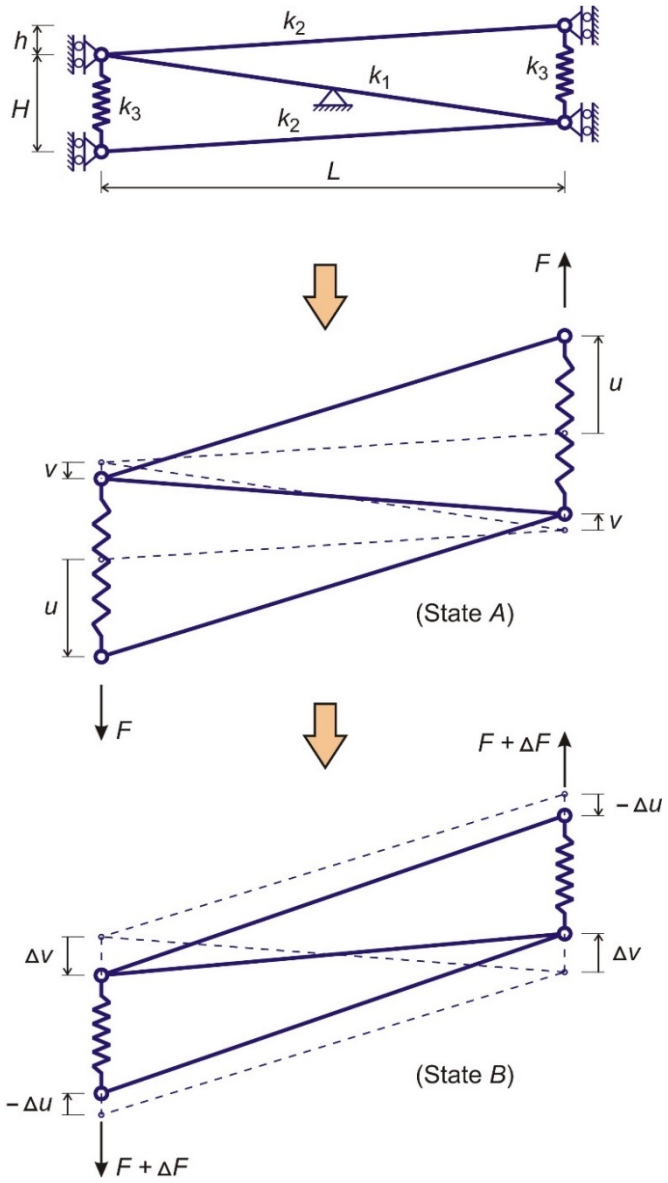

Fig.4: Negative extensibility phenomenon in a five-element bistable structure (unit cell) with linearly elastic members and two independent degrees of freedom, the vertical displacements u and v. L, H and h are dimensions of the unloaded structure at $F = 0$, and k_i are linear stiffnesses of the bar and spring elements. The structure contracts in the direction of applied load when the latter reaches a critical value that destabilizes the structure and induces the transition. This transition is associated with the intermittent rotation of the middle bar "pulling back" on the top and bottom bars of the structure. The negative superelastic strain due to the $A \rightarrow B$ transition is $\varepsilon_{\mathrm{SE}} = -2\Delta u/(H + h)$.

More importantly, using this semi-analytical approach we will show that the negative extensibility is probably a more common phenomenon than previously thought. It may occur for rather simple structures made of several linear elastic links, although at some rare combinations of their physical parameters.

2. Negative Extensibility Phenomenon

Consider a five-element structural unit cell of Fig.4 type, comprised of three inclined bars at moderate deformation and two vertical springs allowing for large elongations. Possible periodic arrangements of such a unit cell in mechanical metamaterials are shown further below in Fig.10.

Using the engineering strain (1) for the springs k_3 and the Green's strain (2) for the bars k_1 and k_2, we can write their strain energies:

$$\pi_1 = \frac{2k_1}{L^2+(H-h)^2} v^2 (v - H + h)^2 \tag{11}$$

$$\pi_2 = \frac{k_2}{8(L^2+h^2)} (u + v)^2 (u + v + 2h)^2 \tag{12}$$

$$\pi_3 = \frac{k_3}{2} (u - v)^2 \tag{13}$$

The total potential energy of the Fig.4 structure is

$$\Pi = \pi_1 + 2(\pi_2 + \pi_3 - Fu) \tag{14}$$

In order to minimize the number of independent system parameters, we may rewrite the potential (14) in terms of the dimensionless quantities:

$$U = a(x + y)^2 (x + y + 2s)^2 + by^2 (y - 1 + s)^2 + (x - y)^2 - 2fx \tag{15}$$

$$U = \frac{\Pi}{k_3 H^2}, \quad f = \frac{F}{k_3 H}, \quad x = \frac{u}{H}, \quad y = \frac{v}{L}; \quad a = \frac{k_2}{4k_3} \frac{H^2}{L^2+h^2}, \quad b = \frac{2k_1}{k_3} \frac{H^2}{L^2+(H-h)^2}, \quad s = \frac{h}{H} \tag{16}$$

By analogy with the equation (6), the dimensionless force *f* is the control parameter, *x* and *y* are two independent state parameters, and *a*, *b* and *s* are the system (design) parameters.

Interestingly, numerical minimization of the potential (15) at certain combinations of the system parameters can provide a pinched hysteresis response with a sought negative extensibility transition. A particularly large contraction at an increasing tensile load was seen at $a = 0.0665$, $b = 5.21$ and $s = 0$, when the $A \to B$ state switching occurred at the critical load $f_C = 1.33$, see Fig.5. The figure shows a numerical solution of the equation (15) using a gradient method, where the force parameter *f* was varied from 0.0 to 1.7 and backward with a step ± 0.001, and the trial solution $x_0 = y_0 = 0.001$ was set initially. Solutions from previous steps were used as trial solutions at further iterations of the force parameter.

We explored Fig.4 type structures of different skewness $s = h/H$ using the analysis to follow and found that the maximal magnitude of the negative extensibility effect has a weak dependence on s in the range from –0.5 to 0.5, and it is better pronounced in *rectangle*-shaped cells. For a concise discussion, we therefore set $s = h = 0$ in (15) and (16), and write the final form of the potential in question:

$$U = a(x+y)^4 + b(y^2-y)^2 + (x-y)^2 - 2fx, \quad a = \frac{k_2}{4k_3}\frac{H^2}{L^2}, \quad b = \frac{2k_1}{k_3}\frac{H^2}{L^2+H^2} \qquad (17)$$

The Fig.5 behavior is qualitatively similar to the negative extensibility observed in some hypothetical atomic systems governed by much more complex potentials [15-17]. We point out, though, on the existence of a secondary (superelastic type) hysteresis at higher loads not mentioned in the earlier publications. We will see below that it should be characteristic to all bistable structures with a negative extensibility transition, and therefore their overall path along the switching equilibrium states could be $A \to B \to A \to B \to A$ in larger amplitude load cycles. Also, simplicity of the potential (17) will enable us to determine an entire range of the system parameters *a* and *b* leading to this remarkable mechanical behavior.

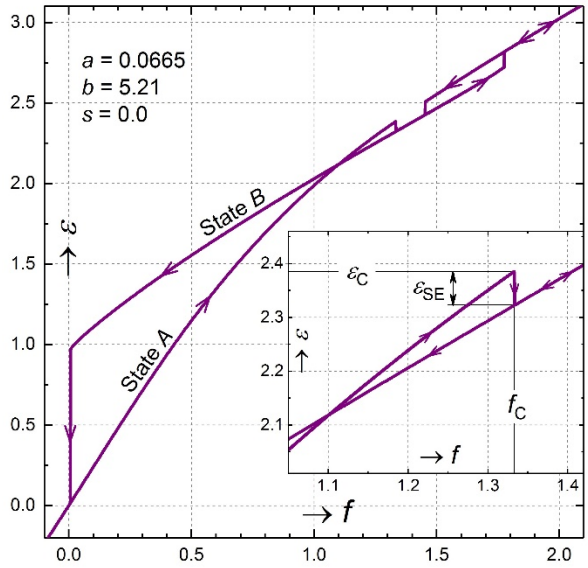

Fig.5: Load-unload cycle of Fig.4 bistable structure governed by the potential (15) or (17) showing a pinched hysteresis and a negative extensibility transition at the critical force $f_C = 1.33$ or critical strain $\varepsilon_C = 2.385$. The negative superelastic strain solely due to the transition, $\varepsilon_{SE} = -0.063$. A secondary hysteresis also exists at the higher loads. States *A* and *B* are two structural *polymorphs* with different stiffnesses. The overall path of load-induced switching between the states is $A \to B \to A \to B \to A$.

3. Structural destabilization and bifurcation points

Stationary points of the scalar potential (17) are defined by the simultaneous conditions

$$U'_x = 0: \quad g_1(x, y, f, a, b) = x - y + 2a(x + y)^3 - f = 0 \tag{18}$$

$$U'_y = 0: \quad g_2(x, y, a, b) = y - x + 2a(x + y)^3 + by(y - 1)(2y - 1) = 0 \tag{19}$$

which correspond to a mechanical equilibrium of the structure. We will refer to these conditions as to the *equilibrium set* conditions. Specific equilibrium states $\{x, y\}$ will depend on the combinations of the control and system parameters $\{f, a, b\}$. The equilibrium set is an intersection of the hypersurfaces g_1 and g_2.

Structural destabilization and switching to a new stable equilibrium configuration occurs in a snap-through action, when the external load reaches some critical value f_C. Mathematically, this corresponds to an *inflection point* singularity on the potential (17), or a *saddle node* bifurcation in the solution space. A necessary mathematical condition for an inflection point can be written in terms of the determinant of the Hessian matrix of second-order derivatives of the potential (17) [20-22],

$$\det H = \begin{vmatrix} U''_{xx} & U''_{xy} \\ U''_{yx} & U''_{yy} \end{vmatrix} = U''_{xx}U''_{yy} - U''_{xy}U''_{yx} = 0: \tag{20}$$

$$g_3(x, y, a, b) = 24a(x + y)^2 + b(6y^2 - 6y + 1)(1 + 6a(x + y)^2) = 0$$

The condition (19) replaces $U''_{xx} = 0$ used in (10) for the analysis of structures with one independent degree of freedom. In an immediate vicinity of a limit point, the structure is in equilibrium, and therefore the criterion for an inflection point (structural destabilization) is the following:

$$g_1(x, y, f_C, a, b) = g_2(x, y, a, b) = g_3(x, y, a, b) = 0 \tag{21}$$

The locus of all the limit points $\{f_C, a, b\}$ satisfying (21) is a 3D surface $\Phi_L(f_C, a, b) = 0$ that we may call the *limit set*. Also, the term *bifurcation set* from the catastrophe theory [20-22] could be used, since $\Phi_L(f_C, a, b) = 0$ contains absolutely all bifurcation points of the potential (17) including the higher order pitchfork bifurcations discussed below. Using the term bifurcation set, one should be aware of a possible confusion; indeed, a bifurcation point in structural analysis is where an equilibrium solution splits rather than jumps.

In a practical sense, the criterion (21) can provide values of the critical (destabilizing) loads f_C for any specific system parameters *a* and *b*. Thus, geometry of the limit set $\Phi_L(f_C, a, b) = 0$ is interesting, although difficult to realize for 2DoF systems, and we will discuss it in more detail in Section 2.2. Note that the limit set geometry for the 1DoF potential (6) was well-represented by the stability diagrams in Fig.3c and Fig.3d showing its two plane cross-sections at some fixed values *a* and *b*.

When the system parameters *a* and *b* are varied in a design process, a stable equilibrium solution $\{x,y\}$ of the equilibrium equations (17) may lose uniqueness at a point of *supercritical pitchfork bifurcation* [23] and split into two stable and one unstable solutions. For the systems with one degree of freedom, this occurred at the *cusp points* (8) within limit set (10) of the potential (6), and these points satisfied the additional condition: $U'''_{xxx} = 0$, see [19] for more details. We

suggest that such a condition should generally apply to an internal degree of freedom responsible for the destabilization. For the Fig.4 structure, this degree of freedom is the rotation of the middle bar k_1 in the plane of the structure, and therefore, we will require

$$U'''_{yyy} = 0: \quad g_4(x, y, a, b) = 24a(x + y) + 12b(2y - 1) = 0 \tag{22}$$

Thus, the criterion for a cusp point (solution splitting) can be written as the following:

$$g_1(x, y, f, a, b) = g_2(x, y, a, b) = g_3(x, y, a, b) = g_4(x, y, a, b) = 0 \tag{23}$$

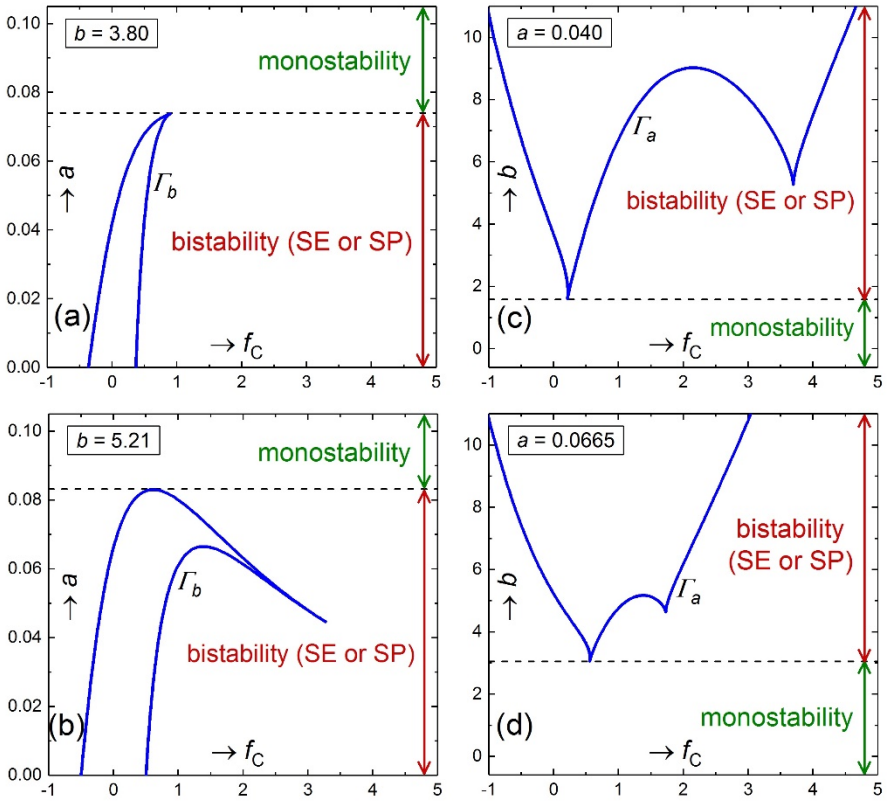

Fig.6: Stability diagrams of Fig.4 bistable structure governed by the potential (17). Up to four critical forces f_C are possible for some selections of the system parameters *a* and *b*. The bistable response can be either superelastic (SE) when the original configuration is fully restored upon load removal, or superplastic (SP) when the recovery requires load reversal, by analogy with Fig.3.

The locus of all the cusp points $\{a,b\}$ satisfying (23) is a plane curve $\Gamma_S(a, b) = 0$, and we will call it the *cusp set*. Individual points $\{a,b\}$ of the cusp set are independent of the load *f*, because a supercritical pitchfork bifurcation is an outcome of design modification, rather loading change as it was for the saddle-node bifurcations (21). Availability of a non-trivial solution to the equation set (23) in the form of an actual plane curve $\Gamma_S(a, b) = 0$ will indicate that the structure can be bistable, as in principle. One may further assume that the curve Γ_S itself should represent a boundary of the bistability region in the *ab*-parameter design space, similar to the 1DoF systems,

see equation (8) and Fig.3a. However, using Fig.4 structure as an example, we will later see that the true onset of bistability in 2DoF systems may correspond to a condition weaker than (23).

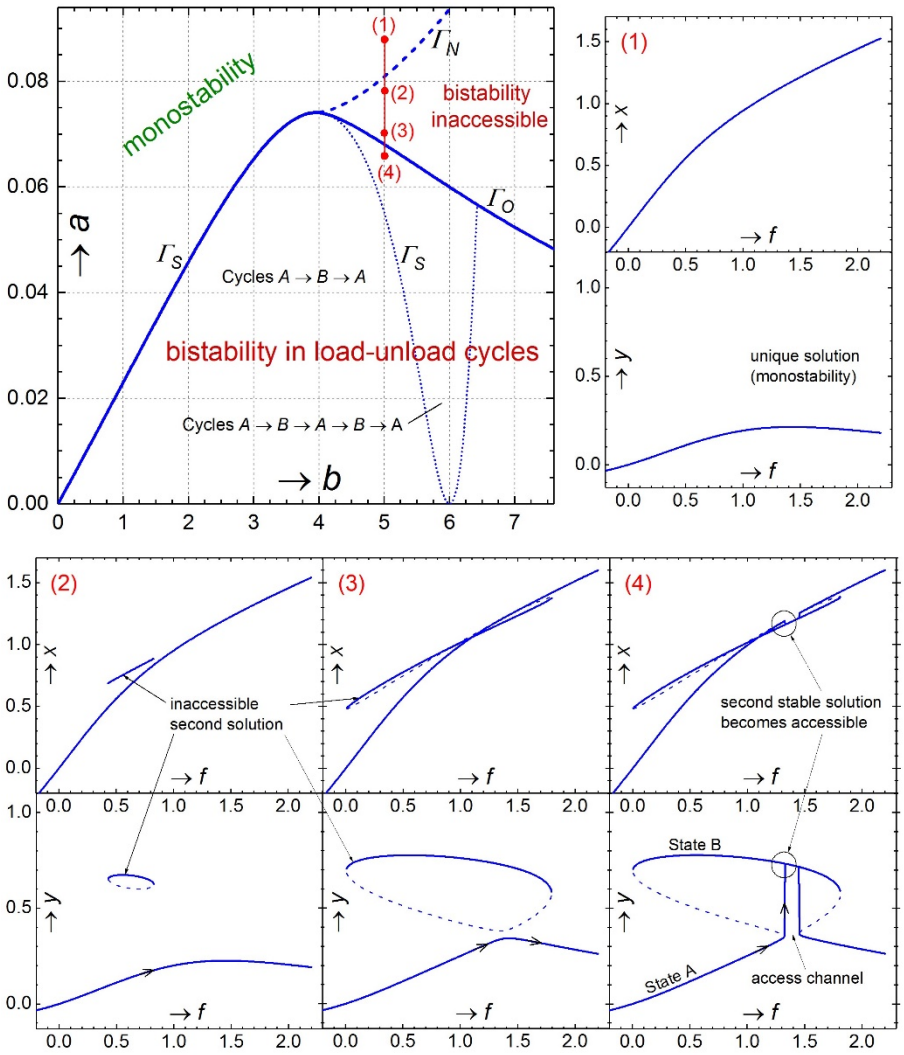

Fig.7: Principal regions of mono- and bistability in the space of design parameters of the potential (17), and a graphical explanation of the second stable solution's nucleation and accessibility change with a decrease of parameter *a* along the line 1-2-3-4. The second stable solution becomes accessible when the new stable-unstable solution loop in the *fy*-plane coalesces with the old solution forming an access channel. The lines Γ_S, Γ_N and Γ_O represent the locus of the cusp, nucleation and coalescence points of the potential (17), accordingly.

3.1 Limit set geometry

For the potential (17), it was possible to derive a unique analytical solution for the limit set equations (21) in terms of $f_C = f_C(y,b)$, $a = a(y,b)$ and also $x = x(y,b)$ via algebraic substitution, see equations (A1-2) in Appendix. Therefore, using y as a varying parameter, we may draw a parametric plane curve $\Gamma_b(f_C, a) = 0$ to represent the (f,a)-*stability diagram* for a given fixed value b. Two examples of it are shown in Fig.6a and Fig.6b. Such a diagram shows a relationship between the system parameter a and the critical loads f_C upon which the switching between two stable equilibrium configurations would occur. It also represents a planar cross-section of the limit set $\Phi_L(f_C, a, b) = 0$ at the fixed value b.

It is also interesting to see a cross-section of the set $\Phi_L(f_C, a, b) = 0$ for a fixed value a, leading to the (f,b)-*stability diagram*. However, for the potential (17), it is not possible to derive an exact algebraic solution for (21) in terms of $f_C = f_C(y,a)$ and $b = b(y,a)$, and we employed a numerical Newton-Raphson iterative procedure for the nonlinear equations set (21) at various instances of y. It was possible to obtain smooth curves, when y varied from 0.22 to 0.78 with a step 0.002. Solutions from previous steps were used as trial solutions for each next iteration of y. Two examples of the curve $\Gamma_a(f,b) = 0$ are shown in Fig.6c and Fig.6d for $a = 0.04$ and 0.0665. Noteworthy, each of these curves contains two cusp points and a local maximum. Therefore, a range of the system parameters a and b exists, at which we can observe switching between the states A and B four times (in the manner $A \to B \to A \to B \to A$) at four different values of the critical force f_C during a *single* load-unload cycle. An example of such a mechanical response was shown earlier in Fig.5.

3.2 Negative extensibility behavior

The most important consequence of the double cusp points mentioned in the previous section is the possibility for a pinch hysteresis required for the negative extensibility behavior. Indeed, values a and b can be selected so that the first transition $A \to B$ leads to a contraction of the structure in the direction of the applied load, see Fig.5. Availability of the four-step transition during a load-unload cycle for an elastic structure seems to be a common feature to accompany the negative extensibility behavior.

3.3 Bistability region clarified

As was mentioned earlier in Section 2.1, a single stable solution to the equilibrium equations may split into two stable and one unstable solutions at a cusp point in the ab-parameter space. For such a special point, four simultaneous conditions (23) must be satisfied. The locus of all the cusp points is the *cusp set*, a plane curve $\Gamma_S(a,b) = 0$. It was possible to get a smooth numerical solution of the equations (23) for the potential (17) in terms of a, f, x and y, depending on the parameter b with the Newton-Raphson method applied to (23) for each specific value of b. The resultant dependence $\Gamma_S(a,b) = 0$ is shown in Fig.7, where b was varied from 0 to 6.5 with a step 0.02.

Some important disclaimers have to be made prior to adopting the curve $\Gamma_S = 0$ in Fig.7 as the onset of bistability. From the bifurcation set geometry discussed in the previous section, we may see that for some values *b*, the bifurcation curve is bent down in a "beak" shape, see Fig.6b. This indicates that the structure may start to demonstrate a bistable behavior (with a decrease of *a*) *earlier* than the cusp point. Indeed, it is sufficient that the value *a* is found lower than the local maximum on the upper branch of the $\Gamma_b(f_C, a) = 0$ curve in Fig.6b. At this point, another pitchfork bifurcation occurs leading to solution splitting into two stable and one unstable configurations. However, the second stable solution nucleates, as shown in Fig.7, to coexist independently in a neighbor region of the solution space inaccessible by the loading of Fig.4 type. It can only be accessed by applying certain coordinated loads to all four nodes of the structure, which is not practical. The points of nucleation of the inaccessible second stable solutions can be determined as those corresponding to the local maximum on the upper branch of the curve $\Gamma_b(f_C, a) = 0$ in Fig.6b, and they are plotted on Fig.7 diagram as the dashed line Γ_N.

As can be seen from Fig.7 plots, this second solution, in a pair with an unstable solution, forms a loop in the *fy*-plane section of the solution space. This loop grows with a decrease of *a*, until it coalesces with the first stable solution, followed by formation of an access channel between them. This channel makes the State *B* accessible in a usual load-unload cycle. The locus of the coalescence points in the *ba*-plane can be determined from the local maximum on the lower branch of the curve $\Gamma_b(f_C, a) = 0$, and they are plotted in Fig.7 diagram as the dashed line Γ_O.

The line of coalescence points, Γ_O, merges with the cusp curve, Γ_S, at $b = 4$ forming a single continuous boundary of the region of the true physical bistability, observable in load-unload cycles of Fig.4 structure. This boundary is shown as the continuous solid line in Fig.7 diagram. In accordance with the stability diagrams of Fig.6, the dotted section of the cusp curve Γ_S below the line Γ_O separates the region of the four-fold switching cycles $A \to B \to A \to B \to A$. We will narrow it to a region of the negative extensibility behavior in the section to follow.

4. Structural Phase Diagram

The plot of Fig.7 is a prototypical phase diagram of the structure showing a boundary between two principal types of structural behavior, bistability and monostability, in the design space. We may now further clarify the behavior subtypes within the bistability region. Since the negative critical forces exist on Fig.6 stability diagrams, the superelastic (reversible on load removal) and superplastic responses should be distinguished, and we also saw a negative extensibility response of the structure in Fig.5 plot. Thus, two more boundary lines should be added to Fig.7 diagram in the region of bistability to complete a structural phase diagram. A region of the Negative Extensibility behavior of SuperElastic type (NESE) will be our primary interest, as leading to the most interesting mechanical metamaterial applications. Continuation of negative extensibility into the superplastic zone

The *elasticity boundary* showing the onset of superelastic behavior, when the structure recovers its original configuration upon load removal, can be determined from the condition that the critical force f_C at the corresponding destabilization point (21) is equal to zero:

$$g_1(x, y, 0, a, b) = g_2(x, y, a, b) = g_3(x, y, a, b) = 0 \qquad (24)$$

A Newton-Raphson procedure was used to solve these equations for a, x and y at each particular value b, which was varied from 0 to 5.21 with a step 0.01. Solutions from the preceding values b were used as trial solutions for the successive values b. The result is a relationship between the parameters a and b given by the curve $\Gamma_E(a, b) = 0$ in Fig.8.

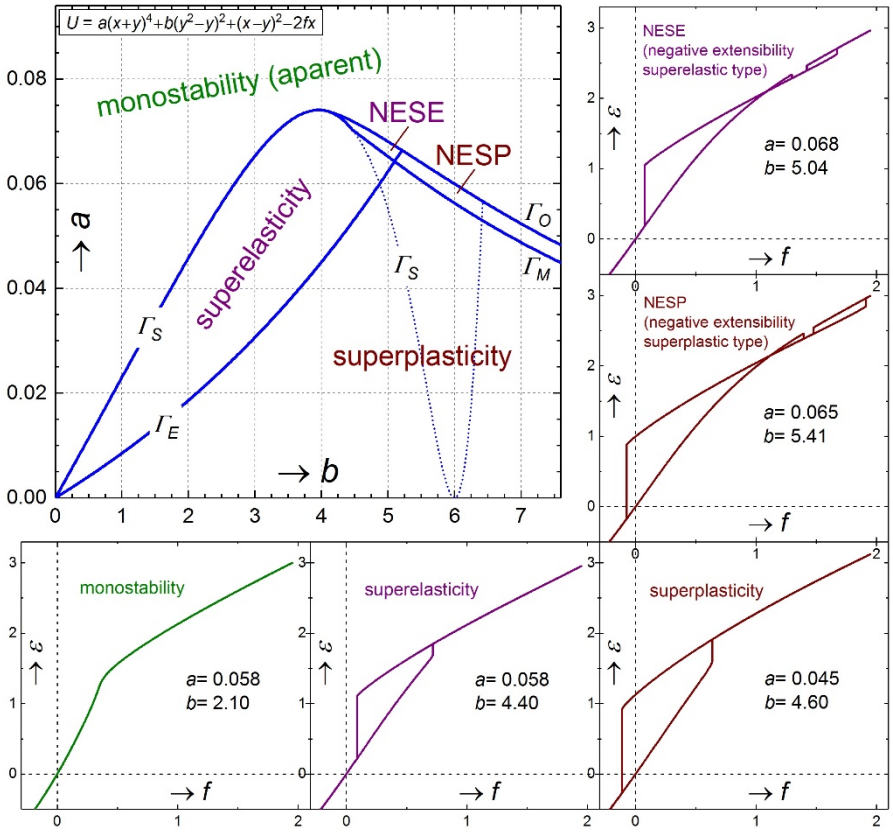

Fig.8: Phase diagram of Fig.4 structure and all mechanical systems governed by the potential $U = a(x + y)^4 + b(y^2 - y)^2 + (x - y)^2 - 2fx$. The most interesting behavior is the negative extensibility of superelastic type (NESE) in a small region of the design space bounded with the curves Γ_O, Γ_M and Γ_E. The region of negative extensibility of superplastic type (NESP) is somewhat larger.

We may now determine the *negative extensibility boundary*, or metastructure behavior boundary showing the onset of the most interesting bistable behavior, when the structure contracts upon tensile load increase as a result of the first transition in the cycle $A \to B \to A \to B \to A$. The formal condition to determine this boundary is the following: the transition $A \to B$ can give a large rotation to the middle bar k_1 of the structure, see Fig.4, while the overall height of the structure must *not* change. We can write this condition as the following,

$$g_1(x_A, y_A, f, a, b) = g_2(x_A, y_A, a, b) = g_3(x_A, y_A, a, b) = 0 \ \wedge$$
$$g_1(x_B = x_A, y_B, f, a, b) = g_2(x_B = x_A, y_B, a, b) = 0 \qquad (25)$$

where x_A and y_A are the values of the state parameters x and y in the configuration A right before the switching, and x_B and y_B are their values right after the switching. These five simultaneous equations can be solved numerically with the Newton-Raphson method for a, f, x_A, y_A, and y_B at a fixed value b. Varying b from 4.5 to 7.5 with a step 0.01 gives a relationship between a and b shown as the curve $\Gamma_M(a, b) = 0$ in Fig.8. As can be seen, the interesting region of NESE (negative extensibility of superelastic type) is bound with the lines Γ_O, Γ_E and Γ_M. The continuation of this region into superplasticity is denoted on phase diagram as NESP (negative extensibility of superplastic type). NESP behavior may also find interesting applications in mechanical shape-memory systems, thermomechanical actuators and impact dampers, alongside with NESE.

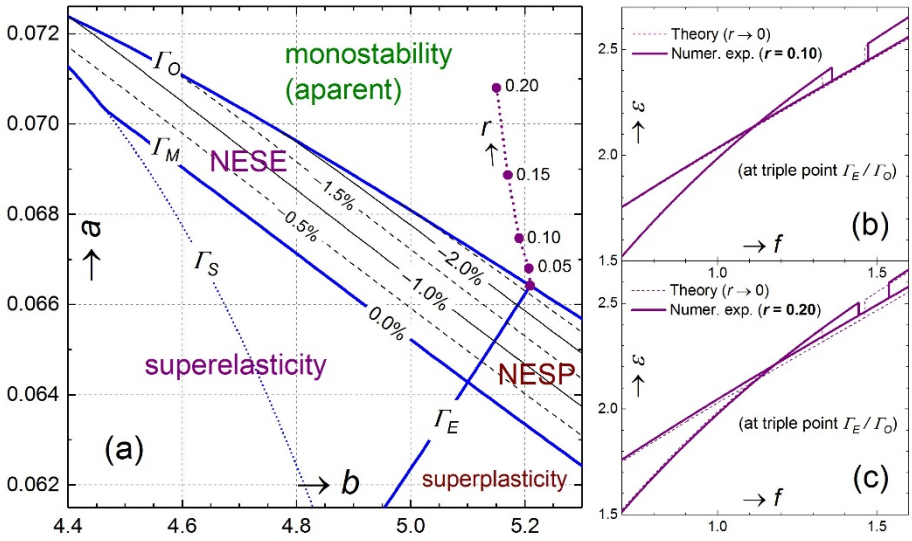

Fig.9: (a) The vicinity of the negative extensibility region of superelastic type (NESE), a zoom of Fig.8 phase diagram. Shown are contour lines of the NESE effect intensity defined in (26). The maximal intensity of –2.64% is observed for the triple point (a = 0.0665, b = 5.21) at the intersection of lines Γ_E and Γ_O. The dotted line marked r shows drift of this point for a structure, governed by the accurate potential (27), with an increase of the structural aspect ratio $r = H/L$. (b-c) Strain-to-load curves of actual structures designed near the triple point at $r = 0.1$ and 0.2, compared to the theoretical prediction discussed in the paper that uses the approximation (4) and corresponds to the limit $r \to 0$.

Finally, we look more closely onto the negative extensibility region and draw the *contour lines* to represent a *relative intensity* of the NESE effect,

$$I_{\mathrm{NESE}} = \varepsilon_{\mathrm{SE}}/\varepsilon_{\mathrm{C}} \qquad (26)$$

where, where ε_{C} is the critical elastic strain and $\varepsilon_{\mathrm{SE}}$ is the negative superelastic strain at the NESE transition $A \to B$, see Fig.5 inset. This parameter describes relative contraction of the structure due to the transition. Noting that the effect intensity is zero along the curve $\Gamma_M(a,b) = 0$, we can relate the dimensionless displacements right before (x_A) and right after (x_B) the transition as the following:

$$x_B = x_A(1 + I_{\mathrm{NESE}}) \tag{27}$$

This condition can be used in (25), instead of $x_B = x_A$, to obtain the contour lines corresponding to various fixed values I_{NESE} with the similar Newton-Raphson iterative procedures. The results are presented in Fig.9, and we may conclude that the maximal effect should be expected in the vicinity of the triple point formed by the superelasticity (Γ_E) and bistability (Γ_O) boundaries.

Figs.7-8 represent together the final phase diagram of Fig.4 structure made of five linearly elastic members, in terms of the dimensionless system (design) parameters *a* and *b* defined in (17). As can be seen, the negative extensibility is a rare behavior occurring only for a small and narrow region in the design space. On the other hand, simplicity of this structure suggests that the negative extensibility is a more ubiquitous property, achievable for a greater range of material systems than previously thought.

5. Error Analysis and Other Parameters

In order to understand the error introduced in the analysis with the Green's strain approximation (4), we define an "accurate" Fig.4 structure potential using only the engineering strain measure (1),

$$\Pi = \pi_1 + 2(\pi_2 + \pi_3 - Fu), \quad \pi_1 = \frac{k_1}{2}\left(\sqrt{L^2 + (H-2v)^2} - \sqrt{L^2 + H^2}\right)^2$$
$$\pi_2 = \frac{k_2}{2}(\sqrt{L^2 + (u+v)^2} - L)^2, \quad \pi_3 = \frac{k_3}{2}(u-v)^2 \tag{28}$$

It is more challenging to perform a systematic analysis of this system, because a dimensionless form of the potential (28) will require three independent system parameters. Indeed, the mechanical behavior will depend also on the *aspect ratio* of Fig.4 structure,

$$r = \frac{H}{L} \tag{29}$$

and the Fig.8 diagram will only represent a cross-section of the 3D design space of the actual structure at $r \to 0$. Thus, the approximation (4) is good at small aspect ratios, when the maximal strain in the bar elements remains low in the hysteretic (bistable) load-unload cycles.

Location of the triple point on the phase diagram representing the maximal NESE effect will drift with *r* in the hypothetical 3D design space as shown in Fig.9 with the dash line. We also found that the greatest discrepancy in the behavior at various $r > 0$ is seen for the critical (switching) force values, see Fig.9b and Fig.9c. All other features of the structural response, including the maximal effect intensity are well reproduced for values *r* up to 0.30. It is safe to

conclude that the approximation (4) and the proposed analysis can provide a starting points for a quick search for the negative extensibility or negative compressibility property in the design space of bistable material systems.

The present methodology is also applicable to other accurate potentials of the type (28), without using the approximation (4), when only two variable system parameters can be identified as interesting ones and other parameters are maintained constant. Several successive procedures of this kind could provide useful planar cross-sections of the corresponding multidimensional design spaces to identify regions of the negative extensibility behavior. For example, several non-zero values of the *skewness* parameter

$$s = \frac{h}{H} \tag{30}$$

of the potential (15) were also considered in range from –0.5 to 0.5. This parameter was found to have a week influence on the maximal achievable NESE effect magnitude, although it was slightly better pronounced in rectangular unit cells.

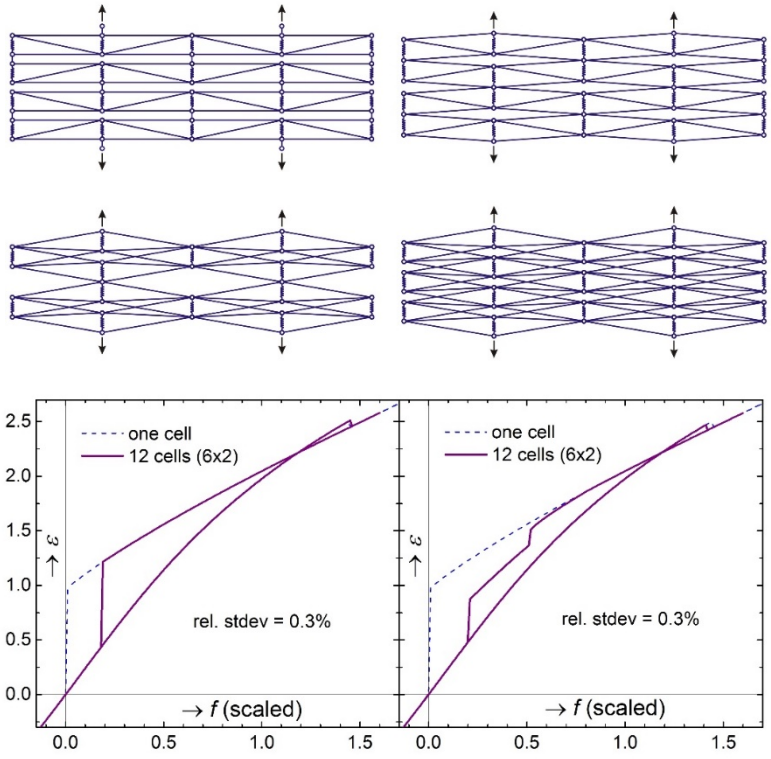

Fig.10: Possible periodic arrangements of NESE cells of Fig.4 type in a periodic mechanical metamaterial or metastructure. Examples of responses observed in imperfect metastructures of the first type (top-left) with random member stiffnesses at relative stdev 0.3%; $a = 0.0708$, $b = 5.15$, $r = 0.2$; periodic boundary conditions are used on the vertical edges, and the loaded nodes are constrained to move synchronically in the vertical direction only; the dash line is the corresponding single-cell response.

6. Conclusions and Outlooks

We discussed the negative extensibility phenomenon in a simple unit cell structure made of 5 non-buckling linearly elastic members, which can be used to fabricate periodic mechanical metamaterials with similar properties. This interesting phenomenon is associated with a special type of bistability transition in the equilibrium solution space of these structures of a more complex type compared to the usual superelastic or superplastic transitions. Simplicity of the unit cell structure studied here suggests that the negative extensibility of superelastic type (NESE), as a highly interesting property of material systems is probably more ubiquitous than earlier thought. It may exist in simple bistable structures with linear material properties, although a thorough analysis would typically be required to identify the relevant suitable ranges of the design parameters for each system type. Furthermore, caution should be taken to avoid losing this property entirely when attempting to increase the effect intensity by approaching (on the phase diagram) the region of apparent monostability, where the bistability is inaccessible in usual load-unload cycles, see Figs.7-8. The reason is the directional nature of negative extensibility property as defined originally in Fig.1. By mental extension of the contour lines in Fig.9 diagram, that region should contain "hidden" negative extensibilities of greater intensities. These behaviors could be unleashed with small additional forces acting on the internal degrees of freedom, and making an interesting mechanical device reminiscent of an electronic switch.

Finally, Fig.10 shows possible arrangements of multiple NESE cells in a periodic metamaterial structure. The collective NESE response of a perfect periodic structure with no randomness in element properties should be equivalent to the unit cell response. However, inevitable small imperfections of elastic member properties in different unit cells may introduce significant deviations from the basic unit cell response. Some of our pilot studies suggest that the critical force value at the NESE transition may shift in both directions, while the reverse transition typically shifts toward the center of the hysteresis, and a step-like character of the transitions can be expected also, see Fig.10. Collective behavior of the bistable periodic NESE medium will certainly have many interesting properties of its own and should be studied more systematically in a separate effort using nonlinear dynamics methods [23-24]. Among these properties are the switching wave propagation speed [24], self-synchronization capabilities, influence of damping components, relaxation transients, effect boundary conditions and loading constrains, and other interesting features. Other simple types of the NESE unit cells should also be sought in the future.

7. Acknowledgements

This work is supported in part by the U.S. National Science Foundation via Grant #1634577.

References

[1] Lakes RS. Foam structures with a negative Poisson's ratio. *Science* 235, 1038–1040, 1987

[2] Hussein MI, Torrent D, Bilal OR. Editorial for the focus issue on Frontiers of Mechanical Metamaterials. *Extreme Mechanics Letters* 12, 1, 2017.

[3] Karpov EG. Structural metamaterials with Saint-Venant edge effect reversal. *Acta Materialia* 123, 245-254, 2017.

[4] Scarpa F, Tomlin PJ. On the transverse shear modulus of negative Poisson's ratio honeycomb structures *Fatigue & Fract. Eng. Mater.* 23, 717–720, 2000.

[5] Grima JN, Caruana-Gauci R, Wojciechowski KW, Evans KE. Smart hexagonal truss systems exhibiting negative compressibility through constrained angle stretching, *Smart Mater. Structures* 22, 084015, 2013.

[6] Yang W, Li ZM, Shi W, Xie BH, Yang MB. Review on auxetic materials. *Journal of Materials Science* 39, 3269-3279, 2004.

[7] Jiang JW, Park HS. Negative Poisson's ratio in single-layer black phosphorus. *Nature Communications* 5, 4727, 2014.

[8] Lim TC. *Auxetic Materials and Structures*, Springer, 2015.

[9] Jiang JW, Kim SY, Park HS. Auxetic nanomaterials: Recent progress and future development. *Applied Physics Reviews* 3, 041101, 2016.

[10] Schenk M, Guest SD. Geometry of Miura-Folded Metamaterials. *PNAS* 110(9), 3276–3281, 2013.

[11] Wei ZY, Guo ZV, Dudte L, Liang HY, Mahadevan L. Geometric Mechanics of Periodic Pleated Origami. *Physical Review Letters* 110, 215501, 2013.

[12] Silverberg JL, Evans AA, McLeod L, Hayward RC, Hull T, Santangelo CD, Cohen I. Using Origami Design Principles to Fold Reprogrammable Mechanical Metamaterials. *Science* 345, 647-650, 2014.

[13] Shan S, Kang S, Zhao Z, Fang L, Bertoldi K. Design of planar isotropic negative Poisson's ratio structures. *Extreme Mechanics Letters* 4, 96-102, 2015.

[14] Shan S, Kang S, Raney JR, Wang P, Fang L, Candido F, Lewis JA, Bertoldi K. Multistable Architected Materials for Trapping Elastic Strain Energy. *Advanced Materials* 27(29). 4296–4301, 2015.

[15] Nicolaou ZG, Motter AE. Mechanical Metamaterials with Negative Compressibility Transitions, *Nature Materials* 11, 608-613, 2012.

[16] Nicolaou ZG, Motter AE. Longitudinal Inverted Compressibility in Super-strained Metamaterials. *J Stat Phys* 151, 1162–1174, 2013.

[17] Chen ML, Karpov EG. Bistability and thermal coupling in elastic metamaterials with negative compressibility. *Physical Review E* 90, 033201, 2014.

[18] Coulais C, Sounas D, Alu A. Static non-reciprocity in mechanical metamaterials. *Nature* 542, 461-464, 2017.

[19] Danso LA, Karpov EG. (http://dx.doi.org/10.1016/j.eml.2017.01.001) Cusp Singularity-Based Bistability Criterion for Geometrically Nonlinear Structures. *Extreme Mechanics Letters*, 2017.

[20] Gilmore R. *Catastrophe Theory for Scientists and Engineers*, Wiley, 1981.

[21] Saunders PT. *An Introduction to Catastrophe Theory*, Cambridge University Press, 1986.

[22] Arnold VI. *Catastrophe Theory*, Springer-Verlag, 1992.

[23] Strogatz SH. *Nonlinear Dynamics and Chaos: With Applications to Physics, Biology, Chemistry, and Engineering*, Westview Press, 2001.

[24] Karpov EG. Bistability, Autowaves and Dissipative Structures in Semiconductor Fibers with Anomalous Resistivity Properties. *Philosophical Magazine* 92(10), 1300–1316, 2012.

Appendix

Analytical solution of the equations (21) for the potential (17):

$$f(y,b)=\frac{by(4-6y+bP_2)}{2P_1},\quad a(y,b)=-\frac{8b(1-6y+6y^2)P_1^2}{27y^2(2+b-3by+2by^2)^2(1+P_1)^3},$$

$$x(y,b)=\frac{y(12+2b(7-24y+18y^2)+3b^2P_2)}{4P_1} \tag{A1}$$

Here, the following notations are used:

$$P_1=3+b-6by+6by^2,\quad P_2=1-9y+26y^2-30y^3+12y^4 \tag{A2}$$